Journal of Magnetic Resonance 209 (2011) 220–226

Contents lists available at ScienceDirect

Journal of Magnetic Resonance

journal homepage: www.elsevier.com/locate/jmr

EPR, optical absorption and superposition model study of Fe^{3+} doped strontium nitrate single crystals

Sangita Pandey, Ram Kripal *

EPR Laboratory, Department of Physics, University of Allahabad, Allahabad 211002, India

ARTICLE INFO

Article history:
Received 30 July 2010
Revised 16 December 2010
Available online 15 January 2011

Keywords:
B. Crystal growth
D. Crystal and ligand fields
D. Optical properties
E. Electron paramagnetic resonance

ABSTRACT

Electron paramagnetic resonance (EPR) study of Fe^{3+} ions doped strontium nitrate (SN) single crystals is performed at liquid nitrogen temperature and at X band frequency. The spin Hamiltonian (SH) parameters are determined from the resonance lines observed at different angular rotations. The crystal field parameters (CFPs) are evaluated using superposition model of Newman. The Zeeman g-factor and zero-field splitting parameters (ZFSPs) of Fe^{3+} ion in SN (truncated SH considered) are: $g = 1.9989 \pm 0.002$ and $|D| = (338 \pm 5) \times 10^{-4}\ cm^{-1}$, $|E| = (10 \pm 5) \times 10^{-4}\ cm^{-1}$, $a = (458 \pm 5) \times 10^{-4}\ cm^{-1}$, respectively. The Fe^{3+} ion enters the lattice substitutionally replacing the Sr^{2+} sites of cubic symmetry. The local site symmetry of Fe^{3+} ion in the crystal is orthorhombic (lower than that of the host). The optical absorption study of the crystal is also done at room temperature in the wavelength range 195–925 nm. The energy values of different orbital levels are determined. The observed bands are assigned as transitions from the $^6A_{1g}(S)$ ground state to various excited states of Fe^{3+} ion in a cubic crystal field approximation. The observed band positions are fitted with four parameters, the Racah interelectronic repulsion parameters (B and C), the cubic crystal field splitting parameter (Dq) and the Trees correction (α) yielding: $B = 934$, $C = 2059$, $Dq = 1450$, and $\alpha = 90$ (in cm^{-1}). On the basis of EPR and optical data, the nature of metal–ligand bonding in this crystal is discussed. The ZFSPs are also determined theoretically using microscopic SH theory based on perturbation theory and CFPs, B_{kq} obtained from superposition model. The values of ZFSPs thus obtained are $|D| = (340 \pm 5) \times 10^{-4}\ cm^{-1}$ and $|E| = (15 \pm 5) \times 10^{-4}\ cm^{-1}$.

1. Introduction

Electron paramagnetic resonance (EPR) study provides information about the local site symmetry and zero-field splitting (ZFS) parameters of transition ions in crystals [1,2]. It is also used to identify the defects responsible for the charge compensation in impurity doped crystals [3]. The optical absorption study is used to find the crystal field strength and the energy level structure of the doped ion [4]. Thus EPR and optical absorption are two supplementary powerful tools to investigate the local environment around the transition ion doped into various crystals, because both of them are very sensitive to distortion of the local lattice structure of the impurity ion. Transition ion doped crystals are important due to their spectroscopic properties making them suitable for laser and optical fiber applications. In the iron group, Fe^{3+} ion is of interest because the $3d^5$ shell, responsible for paramagnetism, is just half filled yielding the resultant angular momentum to be zero in the ground state ^6S with spin $S = 5/2$. The crystalline electric field can affect the electron spins only through high-order interactions, so that the spins are almost completely free to orient themselves in an external magnetic field.

Strontium nitrate, $Sr(NO_3)_2$(SN) is a white granular compound which is used as a precursor for the production of high-purity compounds [5], nanotechnology powders and suspensions [6]. SN is most commonly used in pyrotechnics for the production of red colour, signal lights, marine signals and railroadflares [7]. Due to such applications, the growth and characterization of SN is important.

In the present investigation, the EPR and optical absorption of Fe^{3+} ion in SN are carried out at liquid nitrogen (77 K) and room temperature (300 K), respectively. The purpose of study is to obtain information whether Fe^{3+} ion enters the lattice substitutionally or interstitially, to predict the distortion in the lattice, to find energy separations between different orbital levels, and to describe the nature of bonding of Fe^{3+} ion with its various ligands in the crystal. Theoretical investigations of ZFS parameters are also performed using perturbation theory and crystal field parameters obtained from superposition model [8]. The theoretical results obtained using superposition model are found to be in agreement with the experimental results.

* Corresponding author. Fax: +91 532 2460993.
E-mail addresses: sangitapandey2009@gmail.com (S. Pandey), ram_kripal2001@rediffmail.com (R. Kripal).

1090-7807/$ - see front matter © 2011 Elsevier Inc. All rights reserved.
doi:10.1016/j.jmr.2011.01.014

2. Crystal structure

SN single crystals are cubic with space group $Pa\bar{3}$. The unit cell parameters are $a = b = c = 0.78220$ nm with $Z = 4$ [9,10]. The Sr^{2+} ions form a cubic face centered lattice. They are 12-coordinated by O-atoms, six at a distance of 0.27305 nm and the other six at a distance of 0.28492 nm. The N atoms are located on a threefold rotation axis. They are bonded to three O atoms with a distance of 0.12609 nm. The environment of nitrate group in SN is shown in Fig. 1. The Sr^{2+} sites have cubic symmetry.

3. Experimental

SN single crystals were grown at room temperature by slow evaporation of aqueous solution of strontium nitrate. For Fe^{3+} doped crystals 0.01 mol%. $Fe_2(SO_4)_3$ was added to the aqueous solution. Good colourless crystals of Fe^{3+}:SN were obtained in about 15–20 days. The EPR spectra of the crystals so prepared were recorded at 77 K on Varian X-band E-112 (9.1 GHz) reflection type spectrometer with 100 kHz field modulation. The single crystal was mounted at the end of a quartz-rod using wax and then aligned in TE_{102} cavity center to avoid RF field deterioration. The spectra were recorded as the first derivative of EPR absorption along the three mutually perpendicular crystallographic axes ***a***, ***b*** and ***c*** by rotating the crystal at every 10° using a goniometer.

The optical absorption spectra of Fe^{3+} ion doped SN crystals were recorded on a UNICAM – 5625 – UV/Visible spectrophotometer in the wavelength range 195–925 nm at room temperature.

4. Results and discussion

The recorded EPR spectra for Fe^{3+}:SN crystals at liquid nitrogen temperature when the applied magnetic field **B** is parallel to the '***a***' axis is shown in Fig. 2. For ***B*** in each of the three planes *ab*, *bc* and *ca* a strong broad line is observed. This is assigned to the transition $M = +1/2 \leftrightarrow -1/2$ [11]. In addition, two weak broad lines are also observed at two different orientations (0° and 90°) in the *bc* plane which are assigned to the transitions $M = -3/2 \leftrightarrow -5/2$ and $M = -1/2 \leftrightarrow -3/2$, respectively. No lines corresponding to other transitions were observed even when the magnetic field was scanned up to 0.6 T. The absence of fine structure lines corresponding to other transitions ($M = 3/2 \leftrightarrow 1/2$ and $M = 5/2 \leftrightarrow 3/2$) may be yielding larger linewidth similar to the case of Fe^{3+} in $BaTiO_3$ [12] due to the internal strain. This may also be attributed to small axial ZFS term [13] (discussed later).

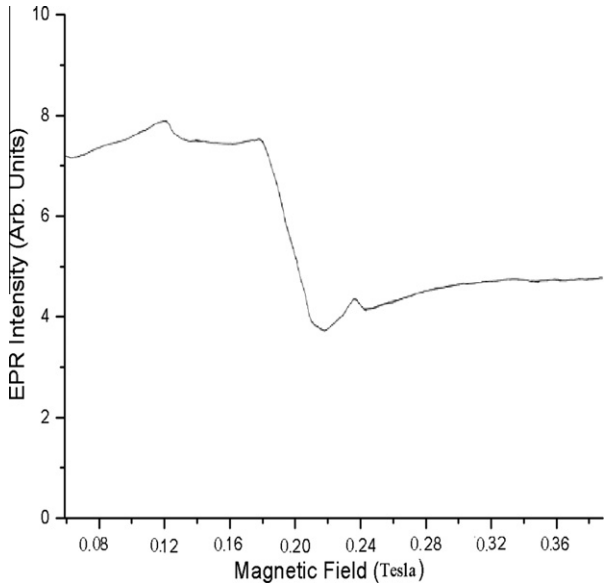

Fig. 2. EPR spectrum of Fe^{3+} ion doped SN single crystals with the magnetic field applied parallel to the **a**-axis.

When Fe^{3+} ion is introduced in SN crystal, it can substitute for Sr^{2+} ions and local site symmetry is reduced to rhombic (lower than that of the host) as is observed in EPR spectra. By the combined effect of crystal field and magnetic interactions [14], the splitting of energy levels of Fe^{3+} ion takes place. The experimental resonance fields are analyzed using the spin Hamiltonian [11,15]

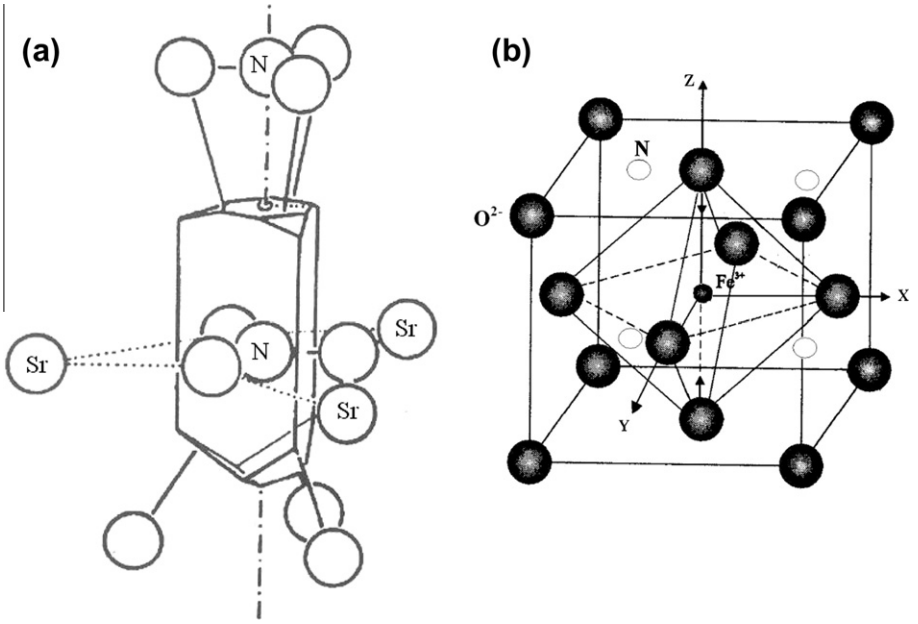

Fig. 1. (a) Environment of the nitrate groups in SN. Unmarked circles denote oxygen atoms (by the courtesy of Nowotny and Heger [8]). (b) Coordination around Fe^{3+} in SN.

$$\mathcal{H} = g\mu_B \boldsymbol{B}\cdot\boldsymbol{S} + D\left\{S_z^2 - \frac{1}{3}S(S+1)\right\} + E\left(S_x^2 - S_y^2\right) + \left(\frac{a}{6}\right)\left[S_x^4 + S_y^4 + S_z^4 - \frac{1}{5}S(S+1)(3S^2+3S-1)\right] + \frac{F}{180} \times \{35S_z^4 - 30S(S+1)S_z^2 + 25S_z^2 - 6S(S+1) + 3S^2(S+1)^2\} + \frac{K}{4}\left[\{7S_z^2 - S(S+1) - 5\}\left(S_+^2 + S_-^2\right) + \left(S_+^2 + S_-^2\right)\{7S_z^2 - S(S+1) - 5\}\right] + AS_zI_z + B(S_xI_x + S_yI_y) \quad (1)$$

where g is the isotropic spectroscopic splitting factor; μ_B, the Bohr magneton; $\boldsymbol{B}$, the external magnetic field. The parameters D and E are the second-rank axial and rhombic ZFS parameters, whereas a, F, and K are the fourth-rank cubic, axial and rhombic ones, respectively. The last two terms in Eq. (1) represent the hyperfine ($I = 5/2$) interaction. The F and K ZFS terms are omitted here as their effect is small [11,16,17]. The isotropic approximation used for the electronic Zeeman interaction is generally valid for $3d^5$ ions [1,11]. The two approximations in question may slightly affect the fitted value of a [18]. The direction of the maximum overall splitting of EPR spectrum is taken as the z axis and that of the minimum as the x axis [19]. The laboratory axes (x,y,z) determined from EPR spectra are found to coincide with the crystallographic axes (CA). The Z-axis of the local site symmetry axes, i.e. the symmetry adapted axes (SAA), is along the metal oxygen bond Sr(1)–O(4) bond in the crystal and the other two axes (X,Y) are perpendicular to the Z-axis (Fig. 1). The allowed transitions and the corresponding resonance fields B for the case of dominant Zeeman interaction are given [11,20] by the equations in Appendix A.

Fig. 3 shows the angular variation of the EPR resonance line, $M = +1/2 \leftrightarrow -1/2$. The values of spin Hamiltonian parameter g, $|D|$, $|E|$ and a obtained using self developed computer program are given in Table 1. The $\boldsymbol{g}$ tensor is calculated at different orientations in all the three planes and then diagonalised using the procedure of Schonland [21] to obtain the principal values: g_x, g_y and g_z. $\boldsymbol{D}$ tensor is calculated by fitting Eq. (A.3) for the transition $M = +1/2 \leftrightarrow -1/2$ to the experimental resonance fields in all three planes ab, bc and ca. The values of $\boldsymbol{D}$ obtained in ab, bc and ca planes are considered to correspond to D_z, D_x and D_y, respectively. Then D and E can be determined by the method given in [15], whereas a is calculated by fitting Eqs. (A.4) and (A.5) for the transitions $M = -1/2 \leftrightarrow -3/2$ and $M = -3/2 \leftrightarrow -5/2$ to the observed resonance fields at two different orientations (0° and 90°) in the bc plane. The directions of the principal axes of the $\boldsymbol{D}$ tensor are nearly the same as that of the $\boldsymbol{g}$ tensor. From Table 1, it is seen that $|D|$ is smaller

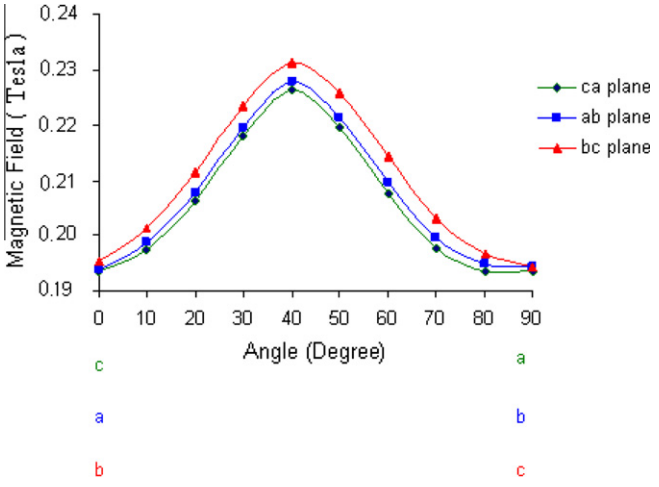

Fig. 3. Angular variation of the EPR spectrum of Fe^{3+}:SN in three planes ca, ab and bc (solid lines represent theoretical plot and symbols are experimental points). ca (c at 0°, a at 90°); ab (a at 0°, b at 90°); bc (b at 0°, c at 90°).

Table 1
Experimental spin Hamiltonian parameters g and D, E, a (in 10^{-4} cm^{-1}) for Fe^{3+} ion in SN together with Fe^{3+} in $BaTiO_3$ single crystals and comparison of theoretical and experimental ZFS parameters for Fe^{3+}:SN.

System	g		$\|D\|$	$\|E\|$	a	
Fe^{3+}:$BaTiO_3$	$g = 2.003$		23		113	[11]
	$g_x = 1.936$	$D_x = 200$	338	10	458	[a]
Fe^{3+}:SN						
	$g_y = 2.002$	$D_y = 220$				
	$g_z = 2.058$	$D_z = 225$				
Theoretical			340	15		

$g = (g_x + g_y + g_z)/3 = 1.999$.
Estimated errors for g, D and a values are ±0.002 and ±5 × 10^{-4} cm^{-1}, respectively.
[a] Present study.

than a (similar to Fe^{3+}: $BaTiO_3$ [12], Table 1) and thus this may be the expected reason of absence of some fine structure lines as mentioned earlier.

To find out whether Fe^{3+} ion enters the SN lattice substitutionally or interstitially, the direction cosines of different bonds are calculated from the crystal structure data (Table 2) and compared with the direction cosines of $\boldsymbol{g}$ obtained from EPR study. The direction cosines of Sr(1)–O(4) bond agree reasonably well with those for the experimental g_z. This indicates that Fe^{3+} ion substitutes at Sr^{2+} site (Fig. 1). Also the ionic radius of Fe^{3+} ion (0.064 nm) [14] is smaller than that of Sr^{2+} ion (0.112 nm) [22]. Thus, Fe^{3+} ion can fit well at the place of Sr^{2+} ion.

This is consistent with the conclusion drawn on the basis of direction cosines. The charge compensation in the crystal is effected either by excess oxygen ions [23] or by vacancies distributed at random throughout the crystal.

5. Optical absorption study

The recorded optical spectra of Fe^{3+} doped SN single crystals at room temperature are given in Fig. 4. The optical spectra consist of 18 bands located at 10916, 11650, 12024, 13793, 14888, 16173, 17839, 18576, 19544, 21403, 22472, 23904, 26746, 32796, 35455, 37412, 39948, and 40789 cm^{-1}. Under cubic site symmetry approximation, the ground state term of Fe^{3+} ion is $^6A_{1g}$ (S). The first four excited multiplets are ^4G, ^4P, ^4D, and ^4F. The shortest wavelength band at 10916 cm^{-1} may be considered due to infrared overtone and/or combination bands (the sum of two or more different wave numbers) [24]. The bands at 11650, 12024 and 13793 cm^{-1} may be the split components of $^6A_{1g}(S) \rightarrow {}^4T_{1g}(G)$ transition [25]. The bands at 14888, 16173, 17839, 18576 and 19544 cm^{-1} are split components of $^6A_{1g}(S) \rightarrow {}^4T_{2g}(G)$ [25]. The sharp bands at 21403 and 26746 cm^{-1} are assigned to $^6A_{1g}(S) \rightarrow {}^4E_g(G)$ and $^6A_{1g}(S) \rightarrow {}^4E_g(D)$ transitions, respectively [25]. The bands at 22472, 23904, 32796 and 35455 cm^{-1} are due to $^6A_{1g}(S) \rightarrow {}^4A_{1g}(G)$, $^6A_{1g}(S) \rightarrow {}^4T_{2g}(D)$, $^6A_{1g}(S) \rightarrow {}^4T_{1g}(P)$ and $^6A_{1g}(S) \rightarrow {}^4A_{2g}(F)$ transitions. The bands at 37412, 39948 and 40789 cm^{-1} may be split components of $^6A_{1g}(S) \rightarrow {}^4T_{1g}(F)$ transition. The two higher wavelength bands corresponding to $^6A_{1g}(S) \rightarrow {}^4A_{2g}(F)$ and $^6A_{1g}(S) \rightarrow {}^4T_{1g}(F)$ transitions are assigned using the energy matrices given by Tanabe and Sugano [26]. The above assignments are consistent with earlier studies [25,26].

The energy levels are evaluated using the Racah parameters (B and C), the cubic crystal field splitting parameter (Dq) and the Trees correction (α). The correction term is relatively small, and so it is arbitrarily fixed at the free ion value of 90 cm^{-1} [27,28]. The parameters B, C and Dq are obtained using equations [29] given in Appendix B.

After assigning the bands, B and C are determined using Eqs. (B.1) and (B.2) and used in solving the secular equations [30] to

Table 2
The ionic distances and direction cosines of different bonds for Fe^{3+}:SN.

Bond	Ionic distances (Å)	Direction cosines with respect to crystallographic axes		
		a	b	c
Sr(1)–O(1)	4.830	±0.4421	±0.4596	±0.7703
Sr(1)–O(2)	2.731	±0.6193	±0.0698	±0.7821
Sr(1)–O(3)	2.849	±0.7792	±0.0669	±0.6232
Sr(1)–O(4)	**8.144**	**±0.2180**	**±0.2726**	**±0.9371**
Sr(1)–N(1)	4.661	±0.5774	±0.5774	±0.5774
Sr(1)–N(2)	3.197	±0.3817	±0.3817	±0.8418
Sr(1)–N(3)	3.197	±0.8418	±0.3817	±0.3817
Sr(1)–N(4)	7.233	±0.1687	±0.3720	±0.9128
[**g**]		**±0.0499**	**±0.9689**	**±0.2422**
		±0.9599	**±0.0204**	**±0.2795**
		±0.2758	**±0.2465**	**±0.9291**

evaluate Dq. The energy values for quartet electronic states have been calculated for different values of Dq with $B = 934\ cm^{-1}$, $C = 2059\ cm^{-1}$ and $\alpha = 90\ cm^{-1}$. A good match of the experimental band positions with the predicted ones is obtained for $Dq = 1450\ cm^{-1}$ as shown in Fig. 5. The band positions and their assignments are given in Table 3. The observed and calculated values are in good agreement, justifying the assignments.

The considerable decrease in the value of the Racah parameters B and C (from 1130 (free ion [31]) to 934, and 4111 to 2059 cm^{-1}) reveals a strong covalent bonding between the central metal ion and the ligands. By analogy with the peak at 407 nm [25] due to Fe^{3+} centre in yttrium aluminium garnet at an octahedral site, the band at 418 nm may be considered as for Fe^{3+}:SN thus confirming Fe^{3+} ion at an octahedral site in SN.

6. Theoretical investigation

In this section, the ZFS parameters (ZFSPs) of Fe^{3+} ion located at Sr^{2+} site in SN are calculated using the microscopic spin Hamiltonian (MSH) theory [15,32]. The crystal-field theory has been extensively applied to the study of the spin Hamiltonian parameters of transition metal ions in crystals [14,33–35]. These works discuss different contributions to ZFSPs and give formulae to determine ZFSPs of the $3d^N$ ions including d^5 ion in terms of the electrostatic, the spin–orbit coupling, and the crystal-field parameters.

For a transition ion in a crystal, the crystal field Hamiltonian can be written as [31].

$$\mathscr{H} = \sum_{k,q} B_{kq} C_q^{(k)} \tag{2}$$

where B_{kq} are the crystal-field parameters and $C_q^{(k)}$ are the Wybourne spherical tensor operators. For the orthorhombic crystal field, $B_{kq} \neq 0$ only with $k = 2, 4$, $q = 0, 2, 4$. Point-charge model and superposition model are generally used to calculate the crystal-field parameters [8,36]. In the present study, we have calculated the crystal-field parameters, B_{kq} using superposition model. This model has been satisfactorily employed for several $3d^n$ ions [14,33–35].

For orthorhombic symmetry, the SO contributions to the ZFS parameters D and E of $3d^5$ ions were derived [37]:

$$D^{(4)}(\mathrm{SO}) = (3\xi^2/70P^2D)\left(-B_{20}^2 - 21\xi B_{20} + 2B_{22}^2\right) + (\xi^2/63P^2G)\left(-5B_{40}^2 - 4B_{42}^2 + 14B_{44}^2\right) \tag{3}$$

$$E^{(4)}(\mathrm{SO}) = (\sqrt{6}\xi^2/70P^2D)(2B_{20} - 21\xi)B_{22} + (\xi^2/63P^2G)(3\sqrt{10}B_{40} + 2\sqrt{7}B_{44})B_{42} \tag{4}$$

where $P = 7B + 7C$, $G = 10B + 5C$, and $D = 17B + 5C$; B and C are the Racah parameters.

By considering the covalency effect via the average covalency parameter N, the B, C and ξ can be expressed in terms of N as [31,38,39],

$$B = N^4 B_0, C = N^4 C_0; \xi_d = N^2 \xi_d^0 \tag{5}$$

where B_0 and C_0, and ξ_d^0 are the free ion Racah and the spin–orbit coupling parameters, respectively [31,39]. For Fe^{3+} ion, the following values are used:

$$B_0 = 1130\ cm^{-1}, C_0 = 4111\ cm^{-1}, \xi_d^0 = 589\ cm^{-1}[31].$$

Using optical study (this work): $B = 934\ cm^{-1}$ and $C = 2059\ cm^{-1}$. Eq. (5) yield $N = 0.953$ and $N = 0.841$, respectively. The average value of $N = 0.897$ is used to calculate the ZFS parameters D and E from Eqs. (3) and (4).

The superposition model expresses the B_{kq} parameters as [37,40]

$$B_{kq} = \sum \overline{A}_k(R_j) K_{kq}(\theta_j, \phi_j) \tag{6}$$

where R_j are the distances between the paramagnetic ion Fe^{3+} and the ligand ion j, R_0 is the reference distance, normally chosen near a value of the R_j's. θ_j are the bond angles in a chosen axis system (preferably SAAS) [8,40]. Summation is taken over all the nearest neighbour ligands. The coordination factors $K_{kq}(\theta_j, \phi_j)$ are the explicit functions of angular position of ligand [8,36,37]. The intrinsic parameter $\overline{A}_k(R_j)$ is given by the power law [37], i.e.

$$\overline{A}_k(R_j) = \overline{A}_k(R_0)(R_0/R_j)^{t_k} \tag{7}$$

where $\overline{A}_k(R_0)$ is the intrinsic parameter for a given ion host system; t_k is power law exponent. For Fe^{3+}–O^{2-} bonds, $t_2 = 3$ and $t_4 = 5$ [31]. For $3d^5$ ions, $\overline{A}_2(R_0)/\overline{A}_4(R_0)$ is 8–12 [41–43]. In the present study, we have taken $\overline{A}_2(R_0)/\overline{A}_4(R_0) = 10$, the middle value of 8 and 12. For $3d^N$ ions in the 6-fold cubic coordination $\overline{A}_4(R_0)$ can be found from the relation [44]: $\overline{A}_4(R_0) = (3/4)Dq$. As $\overline{A}_4(R_0)$ is independent of the coordination [14], we have used above relation to determine $\overline{A}_4(R_0)$ in our calculation. This gives $\overline{A}_4(R_0) = 1087.5\ cm^{-1}$ and $\overline{A}_2(R_0) = 10875\ cm^{-1}$. The values of R_0, R_1, R_1', R_2, R_2'; θ_1, θ_1', θ_2, θ_2'; ϕ_1, ϕ_1', ϕ_2 and ϕ_2' used in the calculation are: 0.1620 nm [45], 0.2849 nm, 0.2849 nm, 0.4830 nm, 0.5935 nm; 90.489°, 94.569°, 84.349°, 97.035°; 51.349°, 4.906°, 46.108° and −6.428°, respectively. There may be considerable covalent bonding between Fe^{3+}–O^{2-}, and thus the reference distance (bond length) R_0 could be smaller than the sum of the ionic radii r_{O2-} (=0.132 nm) and r_{Fe3+} (=0.064 nm). This is partially supported by the data on Ni^{3+} substituting for K^+ in $KTaO_3$ [46] where R_0 is about 0.176 nm which is 0.019 nm smaller than the sum of radii r_{O2-} (=0.132 nm) and r_{Ni3+} (=0.063 nm). Hence, in view of the above, R_0 between Fe^{3+} and O^{2-} is taken as 0.162 nm in our calculation which is 0.034 nm smaller than the sum of radii r_{O2-} (=0.132 nm) and r_{Fe3+} (=0.064 nm). Moreover, Donnerberg et al. [47] obtained correct D value using superposition model with Fe^{3+}–O^{2-} distance about 0.15 nm in Fe^{3+}:$KTaO_3$ system.

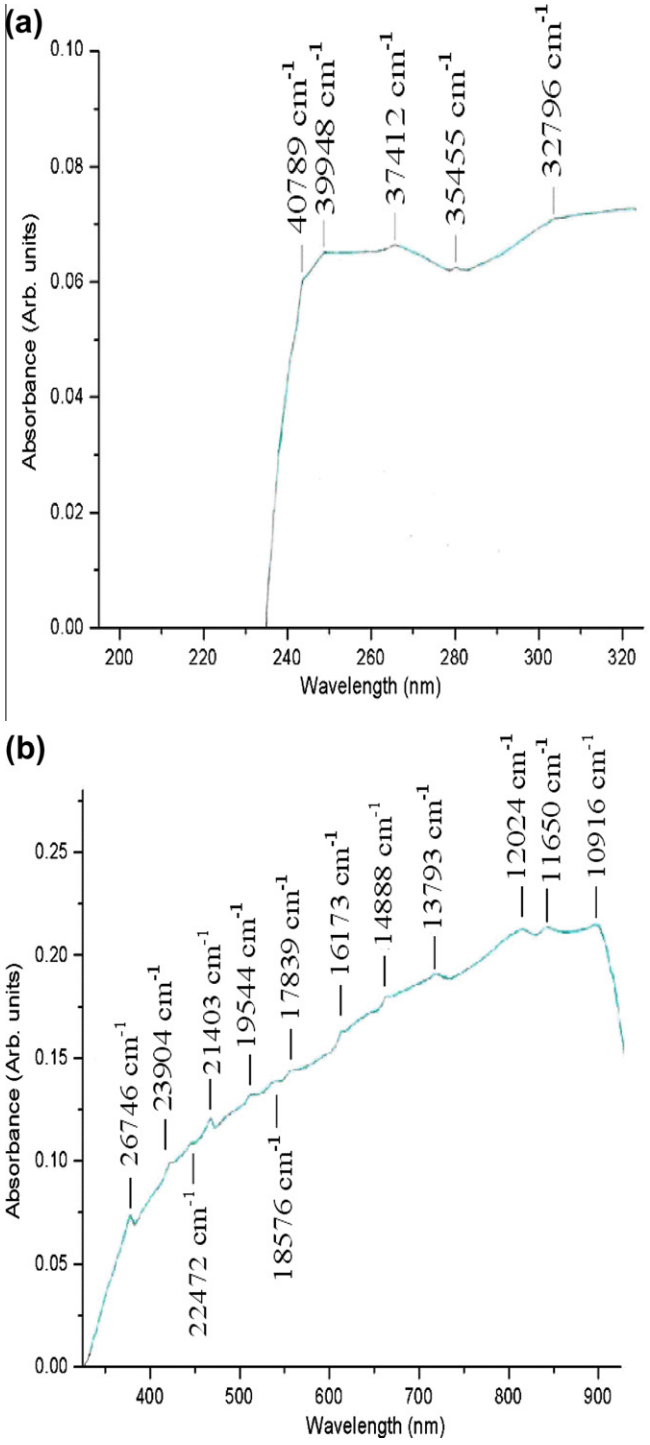

Fig. 4. Optical absorption spectrum of Fe^{3+}:SN at room temperature in the wavelength range (a) 195–325 nm and (b) 325–925 nm.

The crystal-field parameters B_{kq} using Eq. (6) are given [31] in Appendix C. The calculated B_{kq} parameters are obtained (in cm^{-1}): $B_{20} = -224.837$, $B_{22} = -3215.4$, $B_{40} = 0.043$, $B_{42} = 0.835$ and $B_{44} = -1.753$. Using Eqs. (3) and (4) these values of B_{kq} yield the ZFS parameters given in Table 1. The $|D|$ and $|E|$ values thus obtained are in good agreement with the experimental one.

7. Conclusions

EPR study of Fe^{3+} ion doped SN single crystal has been done at 77 K. The spin Hamiltonian parameters (g, $|D|$, $|E|$ and a) have been determined. The results indicate that Fe^{3+} ions enter the lattice substitutionally by replacing Sr^{2+} sites and the charge compensation in the crystal is effected either by excess oxygen ion or by vacancies distributed at random throughout the crystal. The optical absorption study has been carried out at room temperature and the observed bands have been assigned to transitions from the $^6A_{1g}(S)$ ground state to the various excited states of Fe^{3+} ion in cubic crystal field approximation. The Racah parameters (B, C) and crystal field parameter (Dq) have also been evaluated. The considerable decrease in the value of the parameters B and C (from 1130 to 934 and 4111 to 2059 cm^{-1}) shows that there exists a strong covalent bonding between the central metal ion and the ligands. Theoretical investigation of ZFS parameters have also been performed using perturbation formulae and crystal field parameters obtained using superposition model. There is good agreement between the theoretical and experimental results.

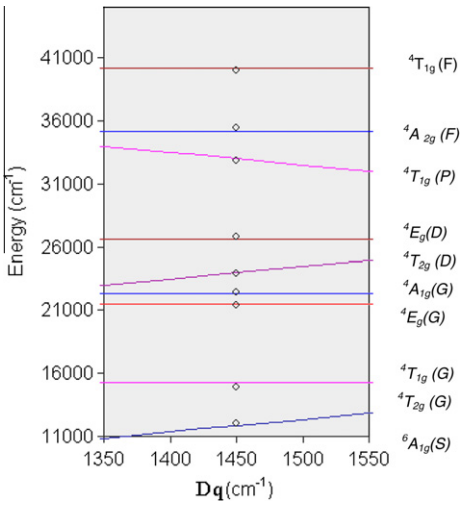

Fig. 5. The energy level diagram of Fe^{3+}:SN showing the variation of the levels with Dq for $B = 934$ and $C = 2059\ cm^{-1}$ (experimental energy values are shown by the circles).

Table 3
Observed and calculated energies of the absorption spectrum of Fe^{3+}:SN; $Dq = 1450$, $B = 934$ and $C = 2059\ cm^{-1}$; uncertainties are given in brackets.

Transition from $^6A_{1g}(S)$	Observed wave number (cm^{-1})	Calculated wave number (cm^{-1})
$^4T_{1g}(G)$	11650 (15)	11827
	12024 (18)	
	13793 (12)	
$^4T_{2g}(G)$	14888 (15)	15283
	16173 (19)	
	17839 (18)	
	18576 (15)	
	19544 (20)	
$^4E_g(G)$	21403 (14)	21483
$^4A_{1g}(G)$	22472 (14)	22369
$^4T_{2g}(D)$	23904 (20)	23972
$^4E_g(D)$	26746 (22)	26590
$^4T_{1g}(P)$	32796 (15)	32976
$^4A_{2g}(F)$	35455 (12)	35108
$^4T_{1g}(F)$	37412 (18)	
	39948 (14)	40170
	40789 (20)	

Acknowledgments

The authors are thankful to the Head, SAIF, I.I.T. Mumbai, Powai, Mumbai for providing the facility of EPR spectrometer. One of the authors, Sangita Pandey is thankful to the Head, Department of

Physics, University of Allahabad, Allahabad for providing departmental facilities.

Appendix A

The allowed transitions and the fields B at which they occur when the Zeeman interaction is dominant as compared with the ZFS terms are given by [11,20]

$$M = +5/2 \leftrightarrow +3/2,$$
$$B = B_0 - 2D(3\mathrm{Cos}^2\theta - 1) - (32D^2/B_0)\mathrm{Cos}^2\theta\mathrm{Sin}^2\theta + (D^2/B_0)\mathrm{Sin}^4\theta - 2pa; \quad (A.1)$$

$$M = +3/2 >\leftrightarrow +1/2,$$
$$B = B_0 - D(3\mathrm{Cos}^2\theta - 1) + (4D^2/B_0)\mathrm{Cos}^2\theta\mathrm{Sin}^2\theta - (5D^2/4B_0)\mathrm{Sin}^4\theta + (5/2)pa; \quad (A.2)$$

$$M = +1/2 \leftrightarrow -1/2,$$
$$B = B_0 + (16D^2/B_0)\mathrm{Cos}^2\theta\mathrm{Sin}^2\theta - (2D^2/B_0)\mathrm{Sin}^4\theta; \quad (A.3)$$

$$M = -1/2 \leftrightarrow -3/2,$$
$$B = B_0 + D(3\mathrm{Cos}^2\theta - 1) + (4D^2/B_0)\mathrm{Cos}^2\theta\mathrm{Sin}^2\theta - (5D^2/4B_0)\mathrm{Sin}^4\theta - (5/2)pa; \quad (A.4)$$

$$M = -3/2 \leftrightarrow -5/2,$$
$$B = B_0 + 2D(3\mathrm{Cos}^2\theta - 1) - (32D^2/B_0)\mathrm{Cos}^2\theta\mathrm{Sin}^2\theta + (D^2/B_0)\mathrm{Sin}^4\theta + 2pa. \quad (A.5)$$

where $B_0 = h\nu/g\mu_B$ and θ is the angle of rotation. The parameter p due to the cubic field is given by the expression $p = (1-5\phi)$, where $\phi = (l^2m^2 + m^2n^2 + n^2l^2)$; (l,m,n) being the direction cosines of magnetic field with respect to the axes (x,y,z).

Appendix B

The electrostatic parameters B and C are calculated from the energy states ${}^4E_g(G)$ and ${}^4E_g(D)$ which are independent of Dq using the energy matrix [29]

$$\begin{vmatrix} -22B + 5C + 12\alpha - E & -2\sqrt{3}B + 4\sqrt{3}\alpha \\ -2\sqrt{3}B + 4\sqrt{3}\alpha & -21B + 5C + 14\alpha - E \end{vmatrix} = 0$$

For the ground state ${}^6A_{1g}(S)$, the energy is $-35B$.

Substituting $E = -35B + T$ in the above equation, we get

$$\begin{vmatrix} 13B + 5C + 12\alpha - T & (-2B + 4\alpha)\sqrt{3} \\ (-2B + 4\alpha)\sqrt{3} & 14B + 5C + 14\alpha - T \end{vmatrix} = 0$$

After solving the above matrix, we get

$$T = 1/2[(27B + 10C + 26\alpha) \pm \sqrt{49B^2 - 188B\alpha + 196\alpha^2}]$$

The solution for the above equation is

$$T_1 = 1/2[(27B + 10C + 26\alpha) - \sqrt{49B^2 - 188B\alpha + 196\alpha^2}]$$
$$T_2 = 1/2[(27B + 10C + 26\alpha) + \sqrt{49B^2 - 188B\alpha + 196\alpha^2}]$$
$$(T_2 - T_1)^2 = [49B^2 - 188B\alpha + 196\alpha^2]$$
$$B = (94\alpha \pm \sqrt{49(T_2 - T_1)^2 - 768\alpha^2})/49$$

In the above expression we always take the positive value of $\sqrt{49(T_2 - T_1)^2 - 768\alpha^2}$.

$$B = (94\alpha + \sqrt{49(T_2 - T_1)^2 - 768\alpha^2})/49 \quad (B.1)$$

Assuming $188 \approx 196$, we have

$$T = 1/2[(27B + 10C + 26\alpha) \pm (7B - 14\alpha)]$$
$$T_1 = 10B + 5C + 20\alpha = {}^4E_g(G)$$
$$T_2 = 17B + 5C + 6\alpha = {}^4E_g(D)$$

Thus,

$$C = (T_1 + T_2 - 27B - 26\alpha)/10 \quad (B.2)$$

As the energy state ${}^4E_g(G)$ lies lower than ${}^4A_{1g}(G)$; we have taken T_1 as ${}^6A_{1g}(S) \rightarrow {}^4E_g(G)$ and T_2 as ${}^6A_{1g}(S) \rightarrow {}^4E_g(D)$.

Appendix C

Relations for the crystal-field parameters derived within the superposition model for the Fe^{3+} ion positioned at the Sr^{2+} site in SN:

$$B_{20} = \overline{A_2}(R_0)\left[(R_0/R_1)^{t_2}(3cos^2\theta_1 - 1) + (R_0/R_1')^{t_2}(3cos^2\theta_1' - 1) + (R_0/R_2)^{t_2}(3cos^2\theta_2 - 1) + (R_0/R_2')^{t_2}(3cos^2\theta_2' - 1)\right] \quad (C.1)$$

$$B_{22} = \sqrt{6}\overline{A}_2(R_0)[(R_0/R_1)^{t_2}sin^2\theta_1 cos(2\phi_1) + (R_0/R_1')^{t_2}sin^2\theta_1' cos(2\phi_1') + (R_0/R_2)^{t_2}sin^2\theta_2 cos(2\phi_2) + (R_0/R_2')^{t_2}sin^2\theta_2' cos(2\phi_2')/2 \quad (C.2)$$

$$B_{40} = \overline{A}_4(R_0)\left[(R_0/R_1)^{t_4}(35cos^4\theta_1 - 30cos^2\theta_1 + 3) + (R_0/R_1')^{t_4}(35cos^4\theta_1' - 30cos^2\theta_1' + 3) + (R_0/R_2)^{t_4}(35cos^4\theta_2 - 30cos^2\theta_2 + 3)\right.$$
$$\left. + (R_0/R_2')^{t_4}(35cos^4\theta_2' - 30cos^2\theta_2' + 3)\right] \quad (C.3)$$

$$B_{42} = \sqrt{10}\overline{A}_4(R_0)\left[(R_0/R_1)^{t_4}sin^2\theta_1(7cos^2\theta_1 - 1)cos(2\phi_1) + (R_0/R_1')^{t_4}sin^2\theta_1'(7cos^2\theta_1' - 1)cos(2\phi_1')\right.$$
$$\left. + (R_0/R_2)^{t_4}sin^2\theta_2(7cos^2\theta_2 - 1)cos(2\phi_2) + (R_0/R_2')^{t_4}sin^2\theta_2'(7cos^2\theta_2' - 1)cos(2\phi_2')\right] \quad (C.4)$$

$$B_{44} = \sqrt{70}\overline{A}_4(R_0)\left[(R_0/R_1)^{t_4}sin^4\theta_1 cos(4\phi_1) + (R_0/R_1')^{t_4}sin^4\theta_1' cos(4\phi_1') + (R_0/R_2)^{t_4}sin^4\theta_2 cos(4\phi_2) + (R_0/R_2')^{t_4}sin^4\theta_2' cos(4\phi_2')\right]/2 \quad (C.5)$$

References

[1] J.A. Weil, J.R. Bolton, Electron Paramagnetic Resonance: Elementary Theory and Practical Applications, second ed., Wiley, New York, 2007.
[2] F.E. Mabbs, D. Collison, Electron Paramagnetic Resonance of d Transition Metal Compounds, Elsevier, Amsterdam, 1992.
[3] J.R. Pilbrow, Transition Ion Electron Paramagnetic Resonance, Clarendon Press, Oxford, 1990.
[4] M. Wildner, M. Andrut, C. Rudowicz, Optical absorption spectroscopy in geosciences, part I: basic concepts of crystal field theory, in: A. Beran, E. Libowitzky (Eds.), Spectroscopic methods in mineralogy, EMU Notes in Mineralogy, vol. 6, Eötvös University Press, Budapest, 2004, pp. 93–143 (Chapter 3).
[5] Y.B. Khollam, S.B. Deshpande, H.S. Potdar, S.V. Bhoraskar, S.R. Sainkar, S.K. Date, Simple oxalate precursor for the preparation of barium–strontium titanate $Ba_{1-x}Sr_xTiO_3$, Mater. Charact. 54 (2005) 63–74.

[6] J. Shao, Y. Tao, J. Wang, C. Xu, W.G. Wang, Investigation of precursors in the preparation of nanostructured $La_{0.6}Sr_{0.4}Co_{0.2}Fe_{0.8}O_{3-\delta}$ via a modified combined complexing method, J. Alloys Compd. 484 (2009) 263–267.
[7] <http://www.skylighter.com/mall/chemicals.asp>.
[8] M. Andrut, M. Wildner, C. Rudowicz, Optical absorption spectroscopy in geosciences, part II: quantitative aspects of crystal fields, in: A. Beran, E. Libowitzky (Eds.), Spectroscopic methods in mineralogy, EMU Notes in Mineralogy, vol. 6, Eötvös University Press, Budapest, 2004, pp. 145–188 (Chapter 4).
[9] B. El-Bali, M. Bolte, $Sr(NO_3)_2$ at 173 K, Acta Cryst. C54 (1998) IUC9800046.
[10] H. Nowotny, G. Heger, Structure refinement of strontium nitrate, $Sr(NO_3)_2$, and Barium nitrate, $Ba(NO_3)_2$, Acta Cryst. C39 (1983) 952–956.
[11] A. Abragam, B. Bleaney, EPR of Transition Ions, Clarendon Press, Oxford, 1970.
[12] T. Sakudo, H. Unoki, Electron spin resonance of Fe^{3+} in $BaTiO_3$ in the rhombohedral and the cubic phases, J. Phys. Soc. Jpn. 19 (1964) 2109–2118.
[13] T. Sakudo, Electron spin resonance of Fe^{3+} in $BaTiO_3$ at low temperature, J. Phys. Soc. Jpn. 18 (1963) 1626–1636.
[14] P. Gnutek, Z.Y. Yang, C. Rudowicz, Modeling local structure using crystal field and spin Hamiltonian parameters: the tetragonal $Fe_K^{3+} - O_I^{2-}$ defect center in $KTaO_3$ crystal, J. Phys.: Condens. Matter 21 (2009) 455402–455412.
[15] C. Rudowicz, Concept of spin Hamiltonian, forms of zero field splitting and electronic Zeeman Hamiltonians and relations between parameters used in EPR. A critical review, Magn. Reson. Rev. 13 (1987) 1–89.
[16] C. Rudowicz, H.W.F. Sung, Can the electron magnetic resonance (EMR) techniques measure the crystal (ligand) field parameters?, Physica B 300 (2001) 1–26
[17] C.J. Radnell, J.R. Pilbrow, S. Subramanian, M.T. Rogers, Electron paramagnetic resonance of Fe^{3+} ions in $(NH_4)_2SbF_5$, J. Chem. Phys. 62 (1975) 4948–4952.
[18] C. Rudowicz, S.B. Madhu, Orthorhombic standardization of spin-Hamiltonian parameters for transition-metal centres in various crystals, J. Phys.: Condens. Matter 11 (1999) 273–287.
[19] C. Rudowicz, R. Bramley, On standardization of the spin Hamiltonian and the ligand field Hamiltonian for orthorhombic symmetry, J. Chem. Phys. 83 (1985) 5192–5197.
[20] B. Bleaney, D.J.E. Ingram, The paramagnetic resonance spectra of two salts of manganese, Proc. Roy. Soc. A205 (1951) 336–356.
[21] D.S. Schonland, On the determination of the principal *g*-values in ESR, Proc. Phys. Soc. 73 (1959) 788–792.
[22] R.C. Weast, CRC Handbook of Chemistry and Physics, 58th ed., CRC Press, Inc., Cleveland, OH, USA, 1977–1978.
[23] W. Low, Paramagnetic resonance and optical absorption spectra of Cr^{3+} in MgO, Phys. Rev. 105 (1957) 801–805.
[24] J.R. Dyer, Applications of Absorption Spectroscopy of Organic Compounds, Prentice Hall of India Pvt. Ltd., New Delhi, 1969.
[25] D. Dong, K.X. Yu, G.J. Jun, W. Hui, Z.K. Wei, Optical absorption and EPR study of the octahedral Fe^{3+} center in yttrium aluminium garnet, Phys. Rev. B 72 (2005) 073101 (1–4).
[26] Y. Tanabe, S. Sugano, On the absorption spectra of complex ions, I, J. Phys. Soc. Jpn. 9 (1954) 753–766.
[27] W. Low, G. Rosengarten, The optical spectrum and ground state splitting of Mn^{2+} and Fe^{3+} ions in the crystal field of cubic symmetry, J. Mol. Spectrosc. 12 (1964) 319–346.
[28] K.X. Yu, C.Z. Hou, Ground-state zero-field splitting for the Fe^{3+} ion in a cubic field, Phys. Rev. B 36 (1987) 797–798.
[29] R. Kripal, V. Mishra, ESR and optical study of Mn^{2+} doped potassium hydrogen sulphate, Solid State Commun. 133 (2005) 23–28.
[30] A.K. Mehra, Tree correction matrices for d^5 configuration in cubic symmetry, J. Chem. Phys. 48 (1968) 4384–4386.
[31] T.H. Yeom, S.H. Choh, M.L. Du, M.S. Jang, EPR study of Fe^{3+} impurities in crystalline $BiVO_4$, Phys. Rev. B 53 (1996) 3415–3421.
[32] C. Rudowicz, S.K. Misra, Spin Hamiltonian formalism in electron magnetic resonance (EMR) and related spectroscopies, Appl. Spectrosc. Rev. 36 (2001) 11–63.
[33] Z.Y. Yang, C. Rudowicz, Y.Y. Yeung, Microscopic spin-Hamiltonian parameters and crystal field energy levels for the low C_3 symmetry Ni^{2+} centre in $LiNbO_3$ crystals, Physica B 348 (2004) 151–159.
[34] Z.Y. Yang, Y. Hao, C. Rudowicz, Y.Y. Yeung, Theoretical investigations of the microscopic spin Hamiltonian parameters including the spin–spin and spin–other–orbit interactions for Ni^{2+} ($3d^8$) ions in trigonal crystal fields, J. Phys.: Condens. Matter 16 (2004) 3481–3494.
[35] T.H. Yeom, Y.M. Chang, S.H. Choh, C. Rudowicz, Experimental and theoretical investigation of spin-Hamiltonian parameters for the low symmetry Fe^{3+} centre in $LiNbO_3$, Phys. Stat. Sol. b185 (1994) 409–415.
[36] C. Rudowicz, On the derivation of the superposition-model formulae using the transformation relations for the Stevens operators, J. Phys. C: Solid State Phys. 20 (1987) 6033–6037.
[37] W.L. Yu, M.G. Zhao, Spin-Hamiltonian parameters of ^6S-state ions, Phys. Rev. B 37 (1988) 9254–9267.
[38] C.K. Jorgensen, Modern Aspects of Ligand Field Theory, North-Holland, Amsterdam, 1971. p. 305.
[39] M.G. Zhao, M.L. Du, G.Y. Sen, A $\mu - \kappa - \alpha$ correlation ligand-field model for the Ni^{2+}–$6X^-$ clusters, J. Phys. C: Solid State Phys. 20 (1987) 5557–5572.
[40] D.J. Newman, B. Ng, The superposition model of crystal fields, Rep. Prog. Phys. 52 (1989) 699–763.
[41] D.J. Newman, D.C. Pryce, W.A. Runciman, Superposition model analysis of the near infrared spectrum of Fe^{2+} in pyrope-almandine garnets, Am. Miner. 63 (1978) 1278–1281.
[42] T.H. Yeom, S.H. Choh, M.L. Du, A theoretical investigation of the zero field splitting parameters for an Mn^{2+} center in a $BiVO_4$ single crystal, J. Phys.: Condens. Matter 5 (1993) 2017–2024.
[43] A. Edgar, Electron paramagnetic resonance studies of divalent cobalt ion in some chloride salts, J. Phys. C: Solid State Phys. 9 (1976) 4303–4314.
[44] D.J. Newman, B. Ng (Eds.), Crystal Field Handbook, Cambridge University Press, Cambridge, 2000.
[45] Y.Y. Yeung, D.J. Newman, Crystal field invariants and parameters for low-symmetry sites, J. Chem. Phys. 82 (1985) 3747–3752.
[46] S.Y. Wu, H.N. Dong, W.H. Wei, Investigation of the spin Hamiltonian parameters and the local structure of two Ni^{3+} centers in $KTaO_3$, Z. Naturf. a59 (2004) 203–208.
[47] H. Donnerberg, M. Exner, C.R.A. Catlow, Local geometry of Fe^{3+} ions on the potassium sites in $KTaO_3$, Phys. Rev. B 47 (1993) 14–19.